

Testing ${}^{6,8}\text{He}$ density distributions by calculations of total reaction cross-sections of ${}^{6,8}\text{He}+{}^{28}\text{Si}$

V.K. LUKYANOV, E.V. ZEMLYANAYA

Joint Institute for Nuclear Research, Dubna 141980, Russia

S.E. MASSEN, Ch.C. MOUSTAKIDIS

Aristotle University of Thessaloniki, Greece

A.N. ANTONOV

Institute for Nuclear Research and Nuclear Energy, Sofia 1784, Bulgaria

G.Z. KRUMOVA

University of Rouse, Rouse 7017, Bulgaria

Abstract

Calculations of the ${}^{6,8}\text{He} + {}^{28}\text{Si}$ total reaction cross sections at intermediate energies are performed on the basis of the Glauber-Sitenko microscopic optical-limit model. The target-nucleus density distribution is taken from the electron-nucleus scattering data, and the ${}^{6,8}\text{He}$ densities are used as they are derived in different models. The results of the calculations are compared with the existing experimental data. The effects of the density tails of the projectile nuclei as well as the role of shell admixtures and short-range correlations are analyzed.

1 Introduction

The study of the matter distributions in the Borromean nucleus ${}^6\text{He}$ and the neutron rich isotope ${}^8\text{He}$ is an actual problem discussed in many papers (see, e.g., in [1] and refs. therein). Investigations give a reason to expect long tails (halo) of the neutron densities. The first result on the enhancement of the strong interaction radii R_I for ${}^{6,8}\text{He}$ was deduced in [2] from measurements of their interaction cross sections with different target nuclei at fixed energy 800 MeV/nucleon. The same conclusion was made in [3] about the ${}^{6,8}\text{He}$ *rms*-radii. Later in [4], the model densities in the form of a sum of two Gaussian functions [5] were fitted to the data and a conclusion for a significant neutron halo in the outer region of these nuclei was made. As to the differential elastic scattering cross sections, they were studied in collisions of ${}^{6,8}\text{He}$ with protons, and the matter distributions of these nuclei were tested using different phenomenological and theoretical models. Elastic scattering angular distributions of ${}^6\text{He} + p$, ${}^6\text{He} + {}^4\text{He}$ ($E_{lab} = 151 \text{ MeV}$) and ${}^6\text{He} + p$, ${}^8\text{He} + p$ ($E < 100 \text{ A MeV}$) were calculated in [6] and [7], respectively, by means of the real part of the optical potentials obtained microscopically by using the realistic M3Y-Paris effective interaction [8, 9, 10] and taking into account the neutron and proton densities of helium isotopes from [4] and also derived from the cluster-orbital shell-model approximation (COSMA) [5],[11],[12],[13]. It was shown in [7] that elastic scattering is a good tool to distinguish between different density distributions. The results of [7] were compared also with those of the alpha-core approach with the fully nonlocal effective interactions [14] and the no-core model based on the large space shell-model calculations (LSSM) [15],[16],[17]. Elastic scattering was recently studied also in [18].

At the same time, small experimental information on the energy dependence of the total reaction cross sections of ${}^{6,8}\text{He}$ with nuclei is available. Generally, from such data for the well-known densities of the target-nuclei, one can get additional constraints on the parameters of

the tested models of the halo nuclei. Below, we present our calculations of the total reaction cross-sections and compare them with the respective data on interactions of ${}^{6,8}\text{He}$ with ${}^{28}\text{Si}$ at energies $E/\text{nucleon} \sim 10 \div 50$ MeV [19, 20].

2 Some formulae

Following [21] we start with the expression for the total reaction cross-sections in the framework of the optical-limit model of the high-energy multiple-scattering theory [22, 23]:

$$\sigma_R = 2\pi \int_0^\infty db b \left(1 - e^{-\chi(b)}\right). \quad (2.1)$$

Here, the eikonal phase for the scattering of the projectile nucleus (p) by the target nucleus (t) is given in [24] by the expression

$$\chi(b) = \bar{\sigma}_{NN} \int d^2s_p d^2s_t \rho_p^\circ(s_p) \rho_t^\circ(s_t) f(\xi), \quad \xi = \mathbf{b} - \mathbf{s}_p + \mathbf{s}_t. \quad (2.2)$$

For the isospin averaged total nucleon-nucleon cross-section $\bar{\sigma}_{NN}$ we use the parametrization from [25]. The vectors \mathbf{s} , ξ are in the impact parameter b plane perpendicular to the z -axis along the relative momentum \mathbf{k}_i of the two scattered nuclei. The thickness densities are given as

$$\rho^\circ(s) = \int_{-\infty}^\infty dz \rho^\circ(\sqrt{s^2 + z^2}), \quad (2.3)$$

where the bare density distributions $\rho^\circ(r)$ of point nucleons in respective nuclei depend on their coordinates in the center-of-mass frames. The function $f(\xi)$ is defined by the form of the nucleon-nucleon interaction amplitude.

To present the phase integral in one-dimensional form, one uses the two-dimensional Fourier-Bessel transformation of all functions in the integrand

$$u(s) = \frac{1}{(2\pi)^2} \int e^{-i\mathbf{q}\mathbf{s}} \tilde{u}(q) d^2q = \frac{1}{2\pi} \int_0^\infty J_0(qs) \tilde{u}(q) q dq, \quad (2.4)$$

where

$$\tilde{u}(q) = \int e^{i\mathbf{q}\mathbf{s}} u(s) d^2s = 2\pi \int_0^\infty J_0(qs) u(s) s ds. \quad (2.5)$$

This results in:

$$\chi(b) = \bar{\sigma}_{NN} \frac{1}{2\pi} \int_0^\infty q dq J_0(qb) \tilde{\rho}_p^\circ(q) \tilde{\rho}_t^\circ(q) \tilde{f}(q). \quad (2.6)$$

The original high-energy scattering theory uses only the transversal component $q_\perp = q \sin \vartheta/2$ of the total momentum transfer $q = 2k \sin \vartheta/2$ and neglects its longitudinal component $q_\parallel = q \cos \vartheta/2$. Here $q^2 = q_\perp^2 + q_\parallel^2$, and k is the momentum of the relative motion.

So, the theory is applied to the scattering angles $\vartheta < \sqrt{2/kR}$, where R is approximately the sum of the radii of both the nuclei¹. So, in eq.(2.6) the use of $q_{\perp} = q$ allows one to take the 3-dimensional Fourier transforms of the functions $\rho^{\circ}(r)$ and $f(\xi)$ instead of the 2-dimensional transforms of their profile functions $\rho^{\circ}(s)$ and $f(s)$. We remind that the form factors of the point $\tilde{\rho}^{\circ}(q)$ and nuclear $\tilde{\rho}(q)$ densities obey the relation

$$\tilde{\rho}(q) = \tilde{\rho}_N(q) \tilde{\rho}^{\circ}(q), \quad (2.7)$$

where the nucleon form factor $\tilde{\rho}_N(q)$ is suggested to be the proton one and has a dipole form which is transformed to the Gaussian function at small q :

$$\tilde{\rho}_N(q) = \left(1 + \frac{q^2 r_{0rms}^2}{12}\right)^{-2} \simeq \exp(-q^2 r_{0rms}^2/6). \quad (2.8)$$

At the same time the form $\tilde{f}(q)$ of the NN-scattering amplitude is known to be

$$\tilde{f}(q) = \exp(-q^2 r_{Nrms}^2/6). \quad (2.9)$$

The squared values of the *rms* radii of the nucleon and the NN-interaction, known from the experimental data as $r_{0rms}^2 = 0.658 fm^2$ and $r_{Nrms}^2 = 0.66 \pm 0.03 fm^2$, almost coincide. It was concluded in [21] that a small difference between these *rms* radii does not influence visibly the calculated total reaction cross sections, and, thus, one can use approximately $\tilde{\rho}_N(q) = \tilde{f}(q)$. Then taking into account Eqs. (2.7)-(2.9) we get the phase (2.6) in a simple form

$$\chi(b) = \bar{\sigma}_{NN} \frac{1}{2\pi} \int_0^{\infty} q dq J_0(qb) \rho_p^{\circ}(q) \rho_t(q). \quad (2.10)$$

The form factors $\rho_t(q)$ can be calculated by using the data on nuclear density distributions. Here, we use the realistic density in the form of the symmetrized Fermi density distribution

$$\rho(r) = \rho_0 \frac{\sinh R/a}{\cosh R/a + \cosh r/a} \simeq \rho_0 \frac{1}{1 + \exp[(r - R)/a]}, \quad (2.11)$$

and the respective form factor obtained in [27] (see also [28]) in the form

$$\tilde{\rho}(q) = -\rho_0 \frac{4\pi a}{q} \frac{d}{dq} \left[\frac{\sin qR}{\sinh \pi a q} \right], \quad \rho_0 = \frac{3A}{4\pi R^3} \left[1 + \left(\frac{\pi a}{R} \right)^2 \right]^{-1}. \quad (2.12)$$

Here R and a are the radius and diffuseness parameters, respectively. Now, taking different models for the projectile nuclei we can test them by comparison of the calculated cross sections with the existing experimental data. Note that if for the densities of the projectile and the target nucleus one takes the Gaussian functions and uses (2.9) for $f(q)$, then the integration in (2.6) can be performed explicitly [21], and one obtains the result of [29] frequently used by experimentalists analyzing experimental data

$$\chi(b) = \bar{\sigma}_{NN} \frac{1}{\pi} \frac{A_p A_t}{a_{G,p}^{\circ 2} + a_{G,t}^{\circ 2} + a_N^2} \exp\left(-\frac{b^2}{a_p^{\circ 2} + a_t^{\circ 2} + a_N^2}\right), \quad (2.13)$$

¹ For estimations of the validity of this approximation one can see [26].

where $a_N^2 = (2/3)r_{N rms}^2$. In the case of the zero-range approximation $a_N = 0$. For the repulsive Coulomb field the trajectory of the incident nucleus deflects from the scattering center. This effect can be taken into account replacing the impact parameter b in the phase $\chi(b)$ by the distance of the closest approach b_c in the Coulomb field

$$b \rightarrow b_c = \bar{a} + \sqrt{\bar{a}^2 + b^2}, \quad (2.14)$$

where $\bar{a} = Z_p Z_t e^2 / 2E_{c.m.}$ is the half-distance of the closest approach at $b = 0$.

In our work, we use models for the projectile nuclei which are known in a table form and, thus, we apply expression (2.10) in the calculations where the density $\rho_t(q)$ of the target nucleus ^{28}Si is taken in a realistic form (2.11) with $R = 3.085 \text{ fm}$ and $a = 0.563 \text{ fm}$ from [30]. The Coulomb distortion effect is also taken into account by using (2.14).

3 Density distributions and calculated cross section

We apply the model for the s-p and s-d shell nuclei, developed in Ref. [31] (M-model), to calculate the $^{6,8}\text{He}$ densities. The densities of these projectile nuclei are used to study the effect of the Jastrow-type short range NN-correlations (SRC), on the total reaction cross-section $^{6,8}\text{He} + ^{28}\text{Si}$ measured at different energies [19, 20].

In the M-model, a general expression for the one-body density matrix of $N = Z$, s-p and s-d shell nuclei [31] has been obtained using the factor cluster expansion method (see Ref.[32] and Refs. therein). That expression depends on the harmonic oscillator (HO) parameter B ($B = (\hbar/(m\omega))^{1/2}$), the occupation numbers A_{nl} of the various states and the correlation parameter β that comes from the Jastrow type correlation function

$$f(r_{ij}) = 1 - \exp[-\beta(r_i - r_j)^2], \quad r_{ij} = |\mathbf{r}_i - \mathbf{r}_j| \quad (3.15)$$

which introduces short range correlations. The effect of correlations introduced by the function $f(r)$ becomes large when the correlation parameter β becomes small and vice versa.

The expression of $\rho(\mathbf{r})$ (in the two body approximation for the cluster expansion) has the form

$$\rho(r) = N [\rho_{SD}^o(r_B) + O_2(r_B, \beta)], \quad r_B = r/B \quad (3.16)$$

where $\rho_{SD}^o(r_B)$, the uncorrelated density distribution corresponding to the Slater determinant HO total wave function, comes from the one-body term of the cluster expansion of the one-body density matrix and the term $O_2(r_B, \beta)$ comes from the two-body term. Their expressions as well as the expression of the normalization factor N are given in [31]. Similar expressions for the form factor and the momentum distribution have also been given in Ref. [31].

The parameters B , β and A_{nl} can be determined, for each nucleus, by fit to the experimental form factors and momentum distributions. As such data are not available for $^{6,8}\text{He}$ we will use the data of the total reaction cross-section and the *rms*-radius. That is, we involve the parameters B , β and the four occupation number A_{1s} , A_{1p} , A_{1d} and A_{2s} in the fitting procedure.

We used as experimental data the well known results of Tanihata et al [4] (T-model) for the density distributions obtained by fit the total reaction cross-section of $^{6,8}\text{He} + ^{12}\text{C}$ at 800 MeV in calculation with the model discussed in Sec. 1, using for the target nucleus

the Gaussian form $\rho_G(r)$ fitted to the realistic density in the outer region and using for the projectile nucleus the harmonic-oscillator form

$$\rho_X^o(r) = \frac{2}{(\tilde{a}\sqrt{\pi})^3} e^{(r/\tilde{a})^2} + \frac{X-2}{3} \frac{2}{(\tilde{b}\sqrt{\pi})^3} \frac{r}{\tilde{b}} e^{(r/\tilde{b})^2}, \quad (3.17)$$

where $X = Z, N$, and \tilde{a}, \tilde{b} are the fitting parameters within the T-model.

Expression (3.17) and the corresponding expression of the *rms*-radius have been used as the "experimental" data of the projectile nuclei ${}^6, {}^8\text{He}$. The values of the parameters B, β and A_{nl} which have been found by a least squares fit of the theoretical neutron and proton density distributions (expression (3.16)) to the "experimental" ones with the constrain that the two densities have the same *rms*-radius are given in Table I. In the case of proton densities there is one free parameter, the HO parameter. For that reason the proton density is taken to be the same for both models.

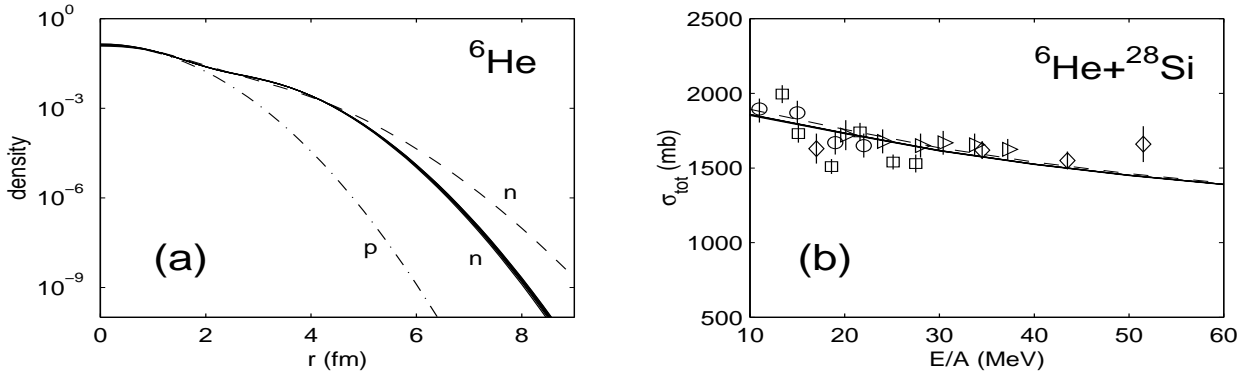


Figure 1: (a) Point density distributions of He-6 calculated using the M-model [17]. Dashed line: neutron density; dash-dotted line: proton density; bold curve is a bundle of eight curves (see the explanations in the text); (b) Total reaction cross section for He-6 + Si-28. The curves are as in a).

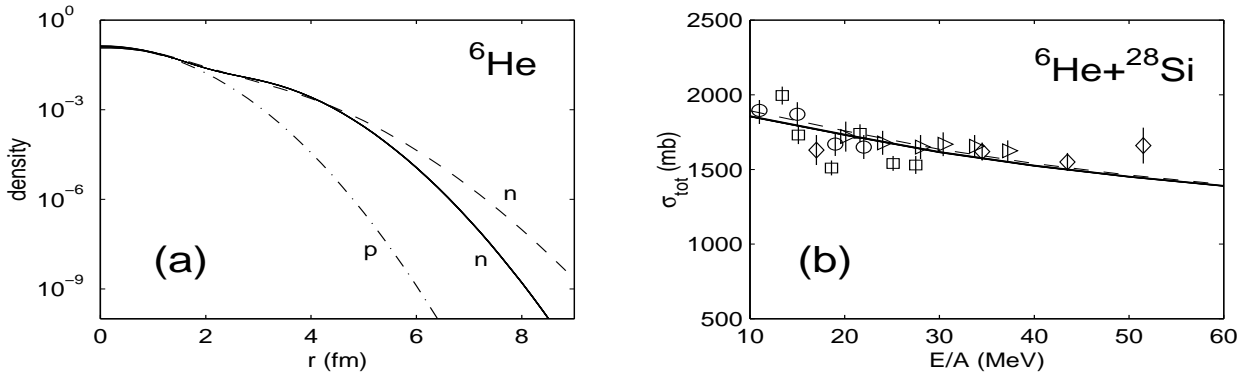


Figure 2: The same as in Fig. 1 from calculations within the M-model [17] where only the parameter beta was used in the fitting procedure.

In order to study the effect of SRC on the density and the total cross section we examined two cases. In the first case we have taken the neutron occupation numbers to be the ones

Table 1: The values of the parameters B , β and A_{nl} , for the neutron and proton densities of ${}^6, {}^8\text{He}$, obtained by fit of the expression (3.16) to expression (3.17) with the constrain that the two densities to give the same *rms*-radius.

Nucleus	$B[\text{fm}]$	$\beta[\text{fm}]^{-2}$	A_{1s}	A_{1p}	A_{1d}	A_{2s}	$R_{rms}[\text{fm}]$
${}^6\text{He}(\text{n})$	1.8249	6.0001	1.9999	1.0889	0.	0.91124	2.5865
${}^8\text{He}(\text{n})$	1.8075	5.1558	2.0000	2.9056	0.	1.0944	2.6587
${}^6\text{He}(\text{p})$	1.53	∞	2.	0.	0.	0.	1.72
${}^8\text{He}(\text{p})$	1.53	∞	2.	0.	0.	0.	1.76

given in Table I, we have given to the correlation parameter β various values from $\beta = 4 \text{ fm}^{-2}$ to $\beta = 50 \text{ fm}^{-2}$ and for each value of β we determined the parameter B so that the neutron *rms*-radius to be the same with the one obtained within the T-model. In figure 1 we present the point density distribution for ${}^6\text{He}$ calculated in this case. The bold curve is the bundle of eight figures. It is seen that the neutron densities of the M-model have lower tails at $r > 5 \text{ fm}$ compared to the one of the T-model. At the same time, we see that the cross-sections are in good coincidence. This means that the main contribution comes from the region $r = 0 \div 5 \text{ fm}$, i.e., up to r equal to about two *rms* radius of the ${}^6\text{He}$ nucleus (the *rms*-radius of the matter distribution is 2.331 fm for both model). From a physical point of view, the increase of the SRC at small β enhances the nuclear radius, but in the considered case one can think that this effect is compensated by reducing the HO parameter B which results in "squeezing" the wave functions of the basis. For that reason we considered the second case where the calculations were made for various values of the parameter β in the range 4 to 50 fm^{-2} while the HO parameter B had the value 1.8249 fm and the parameters A_{nl} were taken as before from Table I. The results are presented in Fig. 2. The calculations in Ref.[31] showed that the changes of the values of β in that region give very significant changes in the form factors and the momentum distributions of nuclei. In the present paper, we study the total cross-sections and as a result, we obtained the corresponding spread of the *rms* radius of the neutron density for ${}^6\text{He}$ in the limit $2.6030 \div 2.5757 \text{ fm}$. However, this does not noticeably influence the cross-sections. Once again, the cross-sections of the M- and the T-models are in coincidence, while the *rms* radii are slightly different.

The same conclusions can be made for ${}^8\text{He}$ nucleus from Figs. 3 and 4, where the results of the calculations within the M-model are presented. In Fig. 3, one can see the bunch of nine curves for the neutron densities when the pairs of the parameters β and B which give the *rms*-radius $R_{rms,n} = 2.6587 \text{ fm}$ are in the regions $\beta = 3.1588 \div 50 \text{ fm}^{-2}$ and $B = 1.7850 \div 1.8261 \text{ fm}$. The occupation numbers are the ones given in Table I. For all the neutron densities the *rms*-radii are in coincidence with the T-model $R_{rms,n} = 2.6857 \text{ fm}$. The matter density radius is also the same in both models $R_{rms,A} = 2.6857 \text{ fm}$. The values of the parameters of the curves in Fig. 4 are: $\beta = 3.1558 \div 10.1558 \text{ fm}^{-2}$, $B = 1.8075 \text{ fm}$ and A_{nl} are the same as in Fig. 3. The obtained values of the *rms* radii of the neutron densities are in the region $2.7172 \div 2.6676 \text{ fm}$. We see that in both figures the slopes of the densities from the M-model begin to differ from that of the T-model at about 5 fm, where the densities fall down by about two orders of magnitude comparing to the values in the nuclear center. Their difference in the range of twice the *rms*-radius does not affect the total cross-sections.

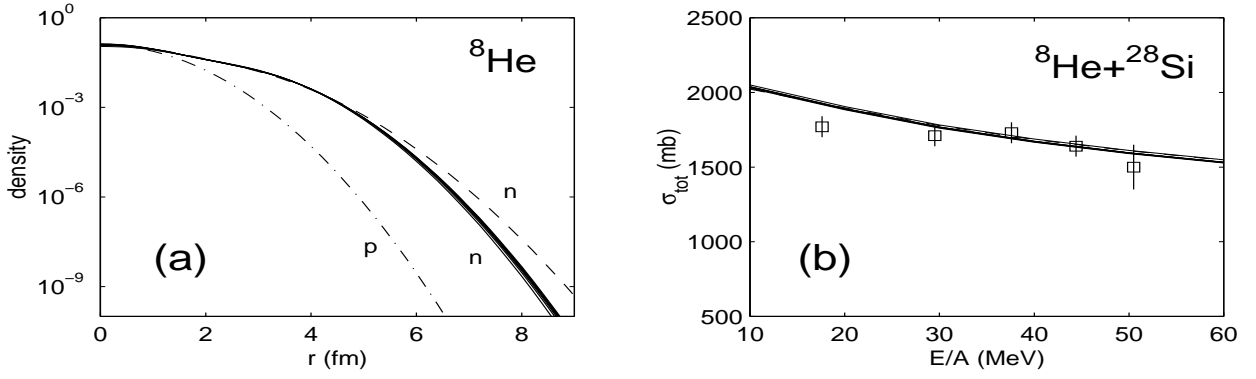


Figure 3: (a) Point density distributions of He-8 calculated using the M-model [17]. Dashed line: neutron density; dash-dotted line: proton density; bold curve is a bundle of neutron densities; (b) Total reaction cross section for He-8+Si-28.

4 Discussion and conclusions

One should mention that in the M-model there were no calculations of the binding energies and the structure of excited states of these nuclei. However, large-scale shell-model calculations (LSSM) of the wave functions and characteristics of light exotic nuclei, such as ${}^6,8\text{He}$ and ${}^9,11\text{Li}$, were reported by several groups, e.g. [17, 33, 34, 35, 36]. They are usually performed by using interactions obtained directly from NN g-matrices with various NN-interactions as their base. In [36], the wave functions for ${}^6,8\text{He}$ were calculated within a complete $4\hbar\omega$ model space by using the g-matrix with interaction from [37]. All calculations were performed by the shell-model code OXBASH [38]. For ${}^4\text{He}$ the harmonic-oscillator single-particle wave functions were used, while for ${}^6,8\text{He}$ they were the Woods-Saxon ones. It was concluded in [36] that ${}^6\text{He}$ corresponds to halo nucleus, while ${}^8\text{He}$ is a neutron skin nucleus. In [5, 13] (and refs. therein), the K-harmonic method was developed and calculations were based on the assumption of the $1p_{3/2}$ state for each of the valence neutrons related to the alpha-core center (COSMA-model). The admixtures of the 3-body forces is included to get the proper value of the binding energy.

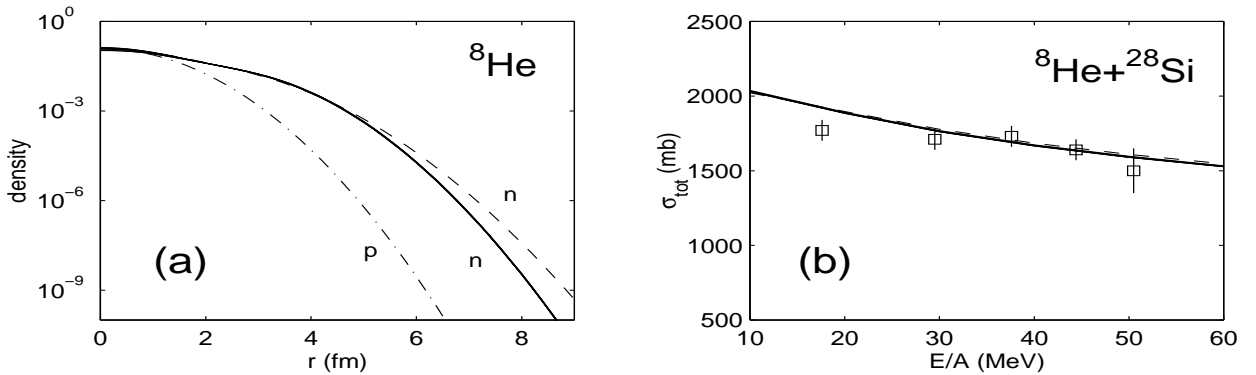


Figure 4: The same as in Fig.3 with differences in the fitting procedure (see the explanations in the text).

In Fig.5, we show the matter density distributions for ${}^6\text{He}$ obtained from the calculations in the framework of the COSMA-model [13] (dash-dots) and the LSSM-model [36] (dots). The M- and T-model densities are shown by the solid bunch and the dashed curve, respectively. First of all, one can see that in the outer region the COSMA- and LSSM-model densities have extended tails which are followed by exponential asymptotics. Here, the dotted curve exceeds the dash-dotted one which results in the enhancement of the corresponding cross section. It is seen that both the cross sections are about $200 \div 500 \text{ mb}$ above those calculated by the M- and T-models and the experimental data. The respective r_{ms} matter radii are $R_{r_{ms},N} = 2.560 \text{ fm}$ (for the dash-dotted curve) and $R_{r_{ms},N} = 2.956 \text{ fm}$ (for the dotted curve). In this connection we refer to [39] where the coupling of elastic and elastic breakup channels were shown to play an important role in processes with weakly bound nuclei, and this can diminish the cross section obtained without accounting for the additional channels. Recently, the theory of the coupled channels was developed in [40, 41] to study the breakup reactions of halo nuclei. In general, the implied optical-limit model needs higher order NN-scattering terms to be included as had been done in the multiple-scattering theory [22, 23]. For example, it was shown in [18] that these terms provide a negative interference and thus diminish the $p + {}^6\text{He}$ differential elastic cross section calculated by taking into account only the single-scattering term. The in-medium effect, which changes the free NN-scattering cross section $\bar{\sigma}_{NN}$ in the phase (2.2) can be included as well. As shown qualitatively in [21], this effect can decrease the total nucleus-nucleus reaction cross sections by about 10%. All the mentioned problems regarding the mechanism of the nucleus-nucleus interaction are still under investigations of the current theory. However, our study of the total reaction cross-sections of the ${}^{6,8}\text{He}$ interactions with the ${}^{28}\text{Si}$ target leads to some general conclusions which, we hope, will not be affected by a possible further modification of the theory.

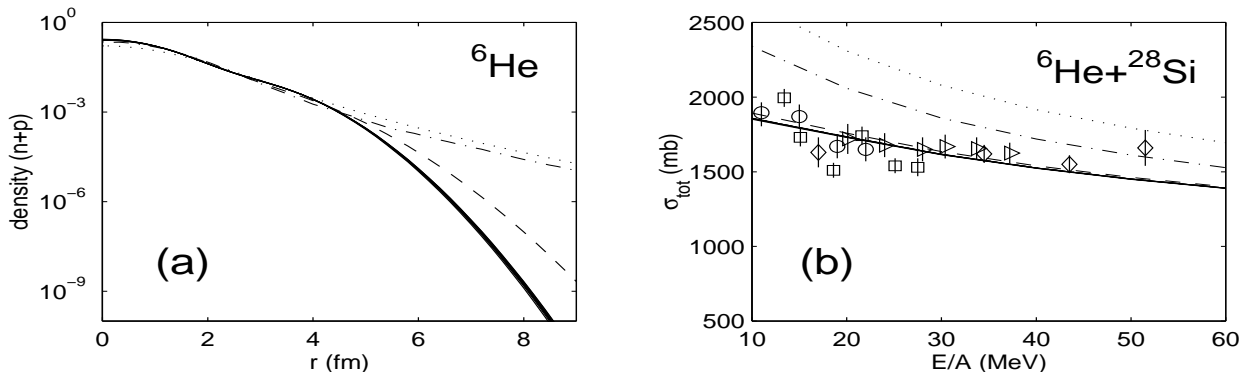


Figure 5: (a) Matter density distributions for He-6 calculated with the COSMA model [21,22] (dash-dotted line) and the LSSM [27] (dotted line). The M- and T-model densities are given by solid bunch and dashed lines, respectively. (b) Total reaction cross section for He-6+ Si-28. The curves are as in (a).

The following conclusions can be drawn from our results:

- The r_{ms} radii are more sensitive nuclear characteristics than the total reaction cross section with respect to changes of the density distributions. The radius depends strongly on variations of the density in the nuclear interior while the behaviour of the

total reaction cross-section depends mainly on the peculiarities of the nuclear surface and weaker on the central nuclear region where strong absorption takes place.

- The previous item explains why variations of the densities due to SRC do not affect the total cross sections while they are significant in calculations of the form factors and of the single-particle momentum distributions in nuclei at large momentum transfers.
- The fitting procedure in our work showed that there is not a $1d$ -shell contribution to the wave functions of ${}^6\text{He}$ and ${}^8\text{He}$.
- In the case of the harmonic-oscillator basis, the Gaussian type of the wave function asymptotics does not affect significantly the cross sections and the latter are formed by taking into account the interior region of the projectile nucleus up to about only two *rms* nuclear radii. Otherwise, if one gets a basis for realistic wave functions, which have an exponential asymptotics, the region of the main contribution becomes larger and achieves the value of about four and larger times the *rms* nuclear radius.

Acknowledgments

The authors would like to thank Dr.S.Ershov for providing the ${}^6\text{He}$ matter density distribution used in investigations in [40, 41]. E.V.Z. was supported by the RFBR under grant No.03-01-00657.

References

- [1] R.F.Casten, B.M.Sherill, *Prog.Part.Nucl.Phys.* **45**, S171 (2000); *see also a special issue of Nucl.Phys.* **A693**, No.1-2 (2001).
- [2] I. Tanihata et al., *Phys.Lett.* **B160**, 380 (1985).
- [3] I. Tanihata et al., *Phys.Rev.Lett.* **55**, (1985) 2676.
- [4] I. Tanihata et al., *Phys.Lett.* **B289**, 261 (1992).
- [5] M.V. Zhukov, A.A. Korshennikov, and M.H. Smedberg, *Phys.Rev.* **C50**, R1 (1994).
- [6] M. Avrigeanu, G.S. Anagnostatos, A.N. Antonov, J. Giapitzakis, *Phys.Rev.* **C62**, 017001 (2000).
- [7] M. Avrigeanu, G.S. Anagnostatos, A.N. Antonov, V. Avrigeanu, *Int.J.Mod.Phys.* **E11**, 249 (2002).
- [8] N. Anantaraman, H. Toki, and G. Bertsch, *Nucl.Phys.* **A398**, 279 (1983).
- [9] R. Satchler and W.G. Love, *Phys.Rep.* **55**, 183 (1979); G.R. Satchler, *Direct Nuclear Reactions* (Clarendon, Oxford, 1983).
- [10] Dao T. Khoa and W. von Oertzen, *Phys.Lett.* **B304**, 8 (1993); *ibid* **B342**, 6 (1995); Dao T. Khoa, W. von Oertzen, and H.G. Bohlen, *Phys.Rev.* **C49**, 1652 (1994); Dao T. Khoa, W. von Oertzen, and A.A. Ogloblin, *Nucl.Phys.* **A602**, 98 (1996); Dao T. Khoa and G.R. Satchler, *Nucl.Phys.* **A668**, 3 (2000).
- [11] A.A. Korshennikov, E.A. Kuzmin, A. Ozawa et al., *Nucl.Phys.* **A616**, 189 (1997).
- [12] A.A. Korshennikov, E.Yu. Nikolskii, C.A. Bertulani et al., *Nucl.Phys.* **A617**, 45 (1997).
- [13] M.V. Zhukov, B.V. Danilin, D.V. Fedorov et al., *Phys.Rep.* **231**, 151 (1993).

- [14] P.J. Dortmans, K. Amos, S. Karataglidis, J. Rainal, *Phys.Rev.* **C58**, 2249 (1998).
- [15] A. Lagoyannis, F. Auger, A. Musnamarra et al., *Phys.Lett.* **B518**, 27 (2001).
- [16] K. Amos, in *Proc. 9th Conf. on Nucl. Reaction Mechanisms, Varenna, 2000*, ed. Ettore Gadioli, (Ricerca Scientifica ed Educazione Permanente, Milano, 2000), p.51.
- [17] S. Karataglidis, B.A. Brown, K. Amos, and P.J. Dortmans, *Phys.Rev.* **C55**, 2826 (1997).
- [18] G.D. Alkharov et al., *Nucl.Phys.* **A712**, 269 (2002);
- [19] R.E. Warner et al., *Phys.Rev.* **C52**, R1166 (1995);
- [20] I.V. Kuznetsov et al., *Yad.Fiz. (Phys.At.Nucl.)* **65**, 1609 (2002);
- [21] V.K. Lukyanov, B. Slowinski, E.V. Zemlyanaya, "Nucleus-nucleus reaction cross-sections calculated for realistic nuclear matter distributions within the Glauber-Sitenko approach", JINR Preprint P4-2003-80, Dubna, 2003; <http://arXiv.org/abs/nucl-th/0308079>.
- [22] R.J. Glauber, *Lectures on Theor. Phys.*, **1**, (Interscience, New York, 1959).
- [23] A.G. Sitenko, *Ukr.Fiz.J.* **4**, 152 (1959).
- [24] W. Czyz, L.S. Maximon, *Ann.of Phys.* **52**, 59 (1969).
- [25] S. Charagi and G.Gupta, *Phys.Rev.* **C41**, 1610 (1990).
- [26] V.K. Lukyanov, E.V. Zemlyanaya, *Int.J.Mod.Phys.* **E10**, no.3, 169 (2001).
- [27] I.Zh. Petkov, V.K. Lukyanov, Yu.S. Pol', *Yad.Fiz.* **9**, 349 (1969).
- [28] M.E. Grypeos, C.G. Koutroulos, V.K. Lukyanov, A.V. Shebeko, *Fiz.Elem.Chast. & At.Yad.* **32**, 1494 (2001); M.E. Grypeos, C.G. Koutroulos, V.K. Lukyanov, A.V. Shebeko, *J. Phys.* **G32**, 779 (2001).
- [29] P.J. Karol, *Phys.Rev.* **C11**, 1203 (1975).
- [30] V.V. Burov, D.N. Kadrev, V.K. Lukyanov, Yu.S. Pol', *Yad.Fiz.* **61**, 595 (1998); V.V. Burov, D.N. Kadrev, V.K. Lukyanov, Yu.S. Pol', *Phys.At.Nucl.* **61**, 525 (1998).
- [31] S.E. Massen, Ch.C. Moustakidis, *Phys.Rev.* **C60**, (1999) 0240005 (1999); Ch.C. Moustakidis, S.E. Massen *Phys.Rev.* **C64**, 014314 (2000).
- [32] J.W. Clark, *Prog.Part.Nucl.Phys.* **2**, 89 (1979).
- [33] P. Navratil and B.R.Barrett, *Phys.Rev.* **C54**, 2986 (1996).
- [34] P. Navratil and B.R. Barrett, *Phys.Rev.* **C57**, 3119 (1998).
- [35] S. Karataglidis, P.G. Hansen, B.A. Brown, K. Amos, and P.J. Dortmans, *Phys.Rev.Lett.* **79**, 1447 (1997); S. Karataglidis, B.A. Brown, K. Amos, and P.J. Dortmans, *Phys.Rev.* **C55**, 2826 (1997).
- [36] S. Karataglidis, P.J. Dortmans, K. Amos, and C. Bennhold, *Phys.Rev.* **C61**, 024319 (2000).
- [37] D.C. Zheng, B.R. Barrett, J.P. Vary, W.C. Haxton, and C.-L. Song, *Phys.Rev.* **C52**, 2488 (1995).
- [38] OXBASH-MSU, the Oxford-Buenos Aires-Michigan State University-shell model code, A. Etchegoyen, W.D.M. Rae, and N.S. Godwin, MSU version by B.A. Brown, 1986; B.A. Brown, A. Etchegoyen, and W.D.M. Rae, MSUCL & nbsp; Report No. 524 , 1986 (unpublished).
- [39] J.S. Al-Khalili, J.A. Tostevin, and I.J. Thompson, *Phys.Rev.* **C54**, 1843 (1996).
- [40] S.N. Ershov, T. Rogde, B.V. Danilin, et al., *Phys.Rev.* **C56**, 1483 (1997).
- [41] S.N. Ershov, B.N. Danilin, J.S. Vaagen, *Phys.Rev.* **C64**, 064609 (2001).